Bioorganic Chemistry 85 (2019) 364–372

Contents lists available at ScienceDirect

Bioorganic Chemistry

journal homepage: www.elsevier.com/locate/bioorg

The mechanism of interactions between flavan-3-ols against *a*-glucosidase and their *in vivo* antihyperglycemic effects

Ling-Ling Zhang[1], Lin Han[1], Shi-Yi Yang, Xue-Mei Meng, Wen-Fang Ma, Min Wang*

College of Food Science and Engineering, Northwest A&F University, 712100 Yangling, PR China

ARTICLE INFO

Keywords:
Flavan-3-ol
A-glucosidase
Inhibition mechanism
Glucose uptake
Intestinal absorption
Postprandial blood glucose

ABSTRACT

Catechin and epicatechin are flavan-3-ols, with (+)-catechin (C) and (−)-epicatechin (EC) being the most common optical isomers found in nature. In this study, we found that C and EC showed notable inhibitory activity against *a*-glucosidase (AGH), and that both inhibition activities reversible and competitive. Additionally, we observed that C and EC quenched the intrinsic fluorescence of AGH through a static quenching mechanism, and that the electrostatic force was the predominant driving factor in the binding reaction. Molecular docking studies indicated that the benzene-ring-4′-hydroxyphenyl construct on flavan-3-ol plays an important role in AGH inhibition, and that the inhibition increases along with increased binding of amino acid residues at this site. Furthermore, C and EC inhibited glucose absorption in everted intestine sleeves *in vitro* and suppressed increases in postprandial blood glucose levels *in vivo*. Our results suggest that C and EC are useful to protect against hyperglycemia through inhibiting the activity of *a*-glucosidase.

1. Introduction

Diabetes represents a group of metabolic diseases characterized by hyperglycemia and that have become increasingly common in recent years [1]. Intensive glycemic control is among the keys to delaying and reducing the complications of diabetes [2]. *a*-Glucosidase (AGH) plays an important role in the absorption of carbohydrates in the human body and based on its ability to hydrolyze carbohydrates into simple absorbable monosaccharides [3]. Therefore, regulating and retarding the activity of key digestive enzymes, such as AGH, can effectively inhibit postprandial hyperglycemia and potentially be used to treat diabetes [4–6]. Synthetic AGH inhibitors, such as acarbose, have been used in clinical practice but are costly and exhibit side effects [3,7–9]. Flavan-3-ols are members of the flavonoid family and that exert antihyperglycemic effects by reducing the absorption of maltose and sucrose in the small intestine [10,11]. (+)-Catechin (C) and (−)-epicatechin (EC) are common flavan-3-ol epimers found in many biologically active natural foods and plants, including chocolate [12], tea [13], and barley [14]. In addition to exhibiting antioxidant and anticancer activities, C and EC display high levels of AGH-inhibitory activities at a low concentration [15]. Yilmazer-Musa et al. [16] previously investigated AGH inhibition by C and EC extracts from natural plants or foods; however, the mechanism of interaction between AGH and its inhibitors remains to be elucidated, and there are no reports describing the antihyperglycemic activity of C and EC *in vivo*.

Here, we performed an in-depth study of the inhibitory effects of flavan-3-ol (C and EC) and an investigation of the mechanism(s) of interaction between C or EC and AGH using enzyme kinetics, fluorescence spectra, energy transfer analysis, atomic force microscope (AFM), and molecular docking. Furthermore, we evaluated AHG inhibition by C and EC in everted intestine sleeves, as well as their ability to lower postprandial blood glucose levels according to sucrose-loading tests *in vivo*.

2. Materials and methods

2.1. Chemicals and reagents

AGH (type I; EC 3.2.1.20; ~50 U/mg) from *Saccharomyces cerevisiae*, *p*-nitrophenyl-α-D-glucopyranoside (*p*NPG), acarbose, C and EC were purchased from Yuanye Biotechnology Co. (Shanghai, China). The stock solutions of AGH (3.0×10^{-6} M) and *p*NPG (3.0×10^{-3} M) were prepared in 0.1 M phosphate-buffered saline (PBS; pH 6.8) for immediate use. C and EC (analytical grade) were dissolved in dimethyl sulfoxide as stock solutions (5×10^{-3} M) and diluted with PBS, as required for experiments. All stock solutions were stored at between

* Corresponding author.
E-mail address: wangmin20050606@163.com (M. Wang).
[1] Ling-Ling Zhang and Lin Han contributed equally to this work.

https://doi.org/10.1016/j.bioorg.2018.12.037
Received 7 November 2018; Received in revised form 26 December 2018; Accepted 28 December 2018
Available online 03 January 2019
0045-2068/

0 °C and 4 °C. All other reagents and solvents were of analytical grade, and ultrapure water was used for all experiments.

2.2. Animals

A total of 10 adult male Sprague–Dawley (SD) rats (200–250 g body weight) and 18 Kunming male mice (30–45 g; SCXK-2017-003) were obtained from the Fourth Military Medical University (Shaanxi, China). All animals were housed at 25 °C maintained with a normal diet, and given access to water *ad libitum*. The experimental protocol was conducted in accordance with the internationally accepted principles for laboratory animal use and care, and the authors further attest that all efforts were made to minimize the number of animals used and their suffering.

2.3. In vitro AGH-inhibition assay

Inhibition of AGH by flavan-3-ol (C/EC) was performed according to a slightly modified method described previously [17–19]. Briefly, AGH (3×10^{-7} M) and *p*NPG (0.3 mM) were prepared in 0.1 M PBS (pH 6.8), and the flavan-3-ol (C/EC) was diluted to different concentrations (0, 0.34, 1.72, 3.45, 17.2, and 34.45×10^{-6} M) using PBS. Acarbose was used as a positive control. For the experiment, 20 μL of acarbose or the inhibitor was pre-incubated with 20 μL of AGH at 37 °C for 15 min. To initiate the reaction, *p*NPG (20 μL) was added to the reaction mixture and incubated at 37 °C for 20 min. The reaction was terminated by adding 120 μL of 0.2 M Na_2CO_3, after which the absorbance at 405 nm was determined using a VICTOR × 3 microplate reader (Perkin Elmer, Waltham, MA, USA). AGH-inhibitory activity was calculated according to the following equation [20]:

$$\%Inhibition = [(A_{20} - A_0) - (S_{20} - S_0)/(A_{20} - A_0)] \times 100$$

where A_{20} and S_{20} are the absorbance of the control and inhibitor, respectively, after 20 min, and A_0 and S_0 are the absorbance of inhibitor and control, respectively, at 0 min.

2.4. Analysis of inhibitory kinetics

Assays were performed in the absence and presence of flavan-3-ol (C/EC) and varying concentrations of AGH (0.3, 0.6, 0.75, and 1.5×10^{-7} M) or substrate (0.3–2.0 mM). The Lineweaver–Burk equation in double-reciprocal form and secondary replots were applied to determine inhibition type [21]. Lineweaver–Burk plots in double-reciprocal form and secondary plots are described by the following equations:

$$\frac{1}{\nu} = \frac{K_m}{\nu_{\max}}\left(1 + \frac{[I]}{K_i}\right)\frac{1}{[S]} + \frac{1}{\nu_{\max}}$$

$$K_m^{app} = \frac{K_m[I]}{K_i} + K_m$$

where K_i and K_m are the inhibition constant and Michaelis–Menten constants, respectively, [I] is the inhibitor concentration, and [S] is the substrate concentration. The secondary plots of slope versus [I] were linearly fitted, in order to identify a single inhibitory site or class of inhibitory sites.

2.5. Mechanism of fluorescence quenching

Fluorescence quenching was used to measure reductions in fluorescence quantum yield caused by intermolecular interactions, such as energy transfer, excitation, and collision quenching [21]. We scaned fluorescence spectra at three different temperatures (298, 304, and 310 K) [22], and titrated by successive addition of 6.8×10^{-4} M diluted C (or EC) solution (resulting in a concentration range of 0–16.17×10^{-6} M) to the AGH solution (1.0×10^{-6} M). Steady state fluorescence-emission spectra were recorded at between 300 nm and 460 nm at an excitation wavelength of 280 nm, with both the excitation and emission slits set to 5.0 nm. Mixtures of enzyme and C (or EC) were equilibrated for 5 min, followed by measurement of fluorescence spectra. The synchronous fluorescence spectra of AGH in the absence and presence of inhibitors were determined by setting the excitation- and emission-wavelength intervals (Δλ) to 15 nm and 60 nm, respectively. To elucidate the probable quenching mechanism between C or EC and AGH, fluorescence quenching was quantified using the Stern–-Volmer equation [23], and the binding constant (K_a) and the number of bound C or EC to AGH (n) were determined by plotting the double logarithm regression curve [21]:

$$F_0/F = 1 + K_q\tau_0[Q] = 1 + K_{sv}[Q]$$

$$\log[(F_0 - F)/F] = n\log K_a - n\log[Q]$$

where F_0 and F are the fluorescence intensity of AGH either with or without inhibitor, respectively, [Q] is the concentration of the inhibitor, K_q and τ_0 (10^{-8} s) represent the bimolecular quenching-rate constant and lifetime of the fluorophore of the enzyme, respectively, K_{sv} and K_a represent the dynamic and static quenching constants, respectively, and n is the number of the binding sites per AGH molecule.

2.6. Fluorescence phase diagram

The fluorescence phase diagram describes the different emission wavelengths (λ_1 and λ_2) used to measure corresponding fluorescence intensities [I (λ_1) and I (λ_2)] when the protein structure changes conformation (unfolded/folded) [24]. We generated this diagram in order to investigate conformational changes in AGH induced by C and EC binding, respectively. We recorded the fluorescence-emission intensities of AGH [I (λ_1) and I (λ_2)] in the presence of different concentrations of C or EC at two specific emission wavelengths [λ_1 (330 nm) and λ_2 (350 nm)], with these expressed by the following equations [22,24] when changes between two different conformations involved an all-or-none transition (relationships will be fitted linearly):

$$I(\lambda_1) = a + bI(\lambda_2)$$

$$a = I_1(\lambda_1) - \frac{I_2(\lambda_1) - I_1(\lambda_1)}{I_2(\lambda_2) - I_1(\lambda_2)}I_1(\lambda_2)$$

$$b = \frac{I_2(\lambda_1) - I_1(\lambda_1)}{I_2(\lambda_2) - I_1(\lambda_2)}$$

where I_1 (λ_1) and I_2 (λ_1) are the fluorescence intensities of the initial and final states of the AGH structure following changes at emission wavelength λ_1, respectively, I_1 (λ_2) and I_2 (λ_2) are the fluorescence intensities of the initial and final states of the AGH structure following changes at emission wavelength λ_2, respectively, and a and b are the intercept and slope of the line, respectively.

2.7. Thermodynamic measurements

Hydrogen bonds, hydrophobic interactions, van der Waals forces, and electrostatic forces are the main driving forces for protein interactions with small molecules. We measured the influence of each inhibitor on fluorescence emission at different temperatures in order to determine changes in enthalpy (ΔH) and entropy change (ΔS), as well as the dominant force exerted between enzyme and inhibitor. Small changes in temperature enable ΔH to be represented as a fixed value. The corresponding ΔH, ΔS, and changes in free energy (ΔG) were calculated using the van't Hoff equation:

$$\log Kb = -\frac{\Delta H}{2.303RT} + \frac{\Delta S}{2.303R}$$

$$\Delta G = \Delta H - T\Delta S$$

where R represents the gas constant (8.314 J mol^{-1} K^{-1}), and T is the

absolute temperature (298, 304, or 310 K).

2.8. Energy transfer analysis

Based on the overlapping spectra of the fluorescence spectrum of AGH and the ultraviolet absorption spectrum of C (or EC), and according to Förster's non-radiative energy transfer theory, the binding-position distance between a small molecule bound to a protein and a tryptophan (Trp) residue within the protein sequence can be determined [25]. The following equation was used to calculate the binding distance (r) associated with the C (or EC) and AGH interaction:

$$E = \frac{R_0^6}{R_0^6 + r^6} = 1 - \frac{F}{F_0}$$

$$R_0^6 = 8.79 \times 10^{-25} \kappa^2 N^{-4} \Phi J$$

$$J = \frac{\sum F(\lambda)\varepsilon(\lambda)\lambda^4 \Delta\lambda}{\sum F(\lambda)\Delta\lambda}$$

where R_0 is the critical distance at $E = 50\%$, κ^2 is the random-orientation factor for AGH and C (or EC), $\kappa^2 = 2/3$, N is the refractive index of the medium ($N = 1.336$), and Φ is the fluorescence quantum yield of AGH ($\Phi = 0.118$) [26]. The overlapping spectral integration between the fluorescence emission spectrum of AGH and the absorption spectrum of the inhibitor is represented by J, and $F(\lambda)$ and $\varepsilon(\lambda)$ are the fluorescence intensity of AGH and the molar absorptivity of C (or EC) at the wavelength of λ, respectively.

2.9. AFM analysis

AFM allows evaluation of changes in protein surface morphology and the distance, particle size, and force magnitude of bound molecules [27]. To investigate the effect of C (or EC) on AGH structure [28], C (or EC; 3.4×10^{-5} M) was added to AGH (20 μL; 6.0×10^{-7} M) and incubated at 37 °C for 20 min, after which the mixture was transferred to a mica substrate and dried at room temperature for 12 h. AFM measurements were determined in air using a Multimode Nanoscop V (Bruker, Billerica, MA, USA), and all images were collected in tapping mode using silicon cantilevers.

2.10. Molecular docking analysis

Molecular docking can help predict the binding of small molecules to enzyme receptors [29]. We used the AGH crystal structure (PDB: 3A4A), and equilibrated the structure following minimization using the Tripos force field, removal of nonpolar water molecules, and the addition of hydrogen atoms and Gasteiger-Huckel charges [29]. The three-dimensional structure of C (or EC) was generated as the ligand, and molecular simulations were performed using Surflex-Dock in Sybyl 2.0 (Certara, Raleigh, NC, USA).

2.11. Measuring sugar absorption on everted intestinal sleeves

Flavan-3-ol (C/EC) inhibition of sugar absorption was assayed on everted intestine sleeves, as previously described [30], in order to evaluate potential *in vivo* activity. Briefly, intestinal segments (3-cm long) from the jejunum 7-week-olds SD rats were weighed, flushed, everted, tied rapidly, and injected with 0.5 mL Ringer's solution. When ready for study, the sleeves were preincubated in glucose-free, mammalian Ringer's solution at 37 °C for 5 min, followed by incubation in Ringer's solution (5 mL) containing sucrose (0.5 mM) and the appropriate concentration of C or EC (0.17–3.46 × 10^{-4} mM). After incubation, glucose concentrations in the soaking solution and intestinal sleeve were tested using a glucose detection kit (Shanghai Rongsheng Biological Pharmaceutical Co., Ltd., Shanghai, China), and the total glucose concentration was calculated. Glucose concentration was defined as glucose per gram of gut weight (mmol/g).

2.12. Oral sucrose load

Sucrose-loading tests were performed using standard non-diabetic Kunming mice after a 12-h food-deprivation period. A solution of sucrose (2 g/kg body weight) together with the appropriate amount of C or EC (20 mg/kg body weight) being evaluated was administered to the mice, with acarbose administered as a positive control at 20 mg/kg. Blood samples were collected via the tail vein and tested at 0, 15, 30, 60, 90, and 120 min after administration using a OneTouch SelectSimple blood glucose meter (Johnson and Johnson Medical Equipment Co., Ltd., Smithfield, NC, USA).

2.13. Statistical analysis

IC_{50} values were estimated by nonlinear curve fitting and presented as their respective 95% confidence intervals. All enzymatic assays were performed in triplicate, and results are expressed as the mean ± standard deviation. Data were analyzed by one-way analysis of variance, followed by multiple tests using the SPSS statistical package (v18.0 for Windows; SPSS, Inc., Chicago, IL, USA). A $p < 0.05$ was considered significant.

3. Results and discussion

3.1. Inhibition of mammalian AGH by flavan-3-ol

C, EC, and acarbose (Fig. 1A) were tested for their ability to inhibit AGH activity. Acarbose (positive control) showed an IC_{50} value of 1250.11 ± 35.63 μM, and Fig. 1B shows the strong inhibitory activities of different concentrations of flavan-3-ol (C and EC) on AGH (IC_{50}: 1.12 ± 0.03 μM and 0.95 ± 0.02 μM, respectively). Previous studies reported the AGH inhibition was closely related to the number and location of hydroxyl groups on the A, B, and C rings of polyphenols, with the 5,6,7-trihydroxyflavone structure of the A-ring critical to this activity, and hydroxyl substitution on the B ring favorable to inhibition [31]. Additionally, a recent study showed that the C-ring structure of flavan-3-ols enhances their inhibition of AGH [32]. As the simplest structural unit constituting flavan-3-ols, EC is the conformational isomer to C. Due to their structural similarity, the inhibitory activities of C and EC are both highly similar and significantly greater than that of acarbose.

We generated plots of υ versus [AGH] for C and EC and at different concentrations (Fig. 1C and D, respectively), revealing a good linear relationship, with the slope of the line gradually decreasing along with increasing C and EC concentrations. These results indicated that the inhibitory effect of C and EC on AGH was reversible.

3.2. Enzyme kinetics study

We then evaluated the degree and type of inhibition exerted by C and EC on AGH, with the results presented as Lineweaver–Burk double-reciprocal plots and secondary plots. The results showed similar υ_{max} and different *Km* values between C and EC binding to AGH, suggesting C (Fig. 1E) and EC (Fig. 1F) as competitive inhibitors bound only to free enzyme. Re-plot of the two inhibitors at different concentrations (according to K_{mapp} values) revealed good linear fits and confirmed the presence of a single inhibition site on the enzyme. Additionally, K_i values were calculated at 1.47 ± 0.02 × 10^{-5} M (C) and 2.04 ± 0.03 × 10^{-5} M (EC).

3.3. Fluorescence quenching of AGH.

Fluorescence measurements reflect the degree of small-molecule binding to proteins and allow elucidation of binding mechanisms and

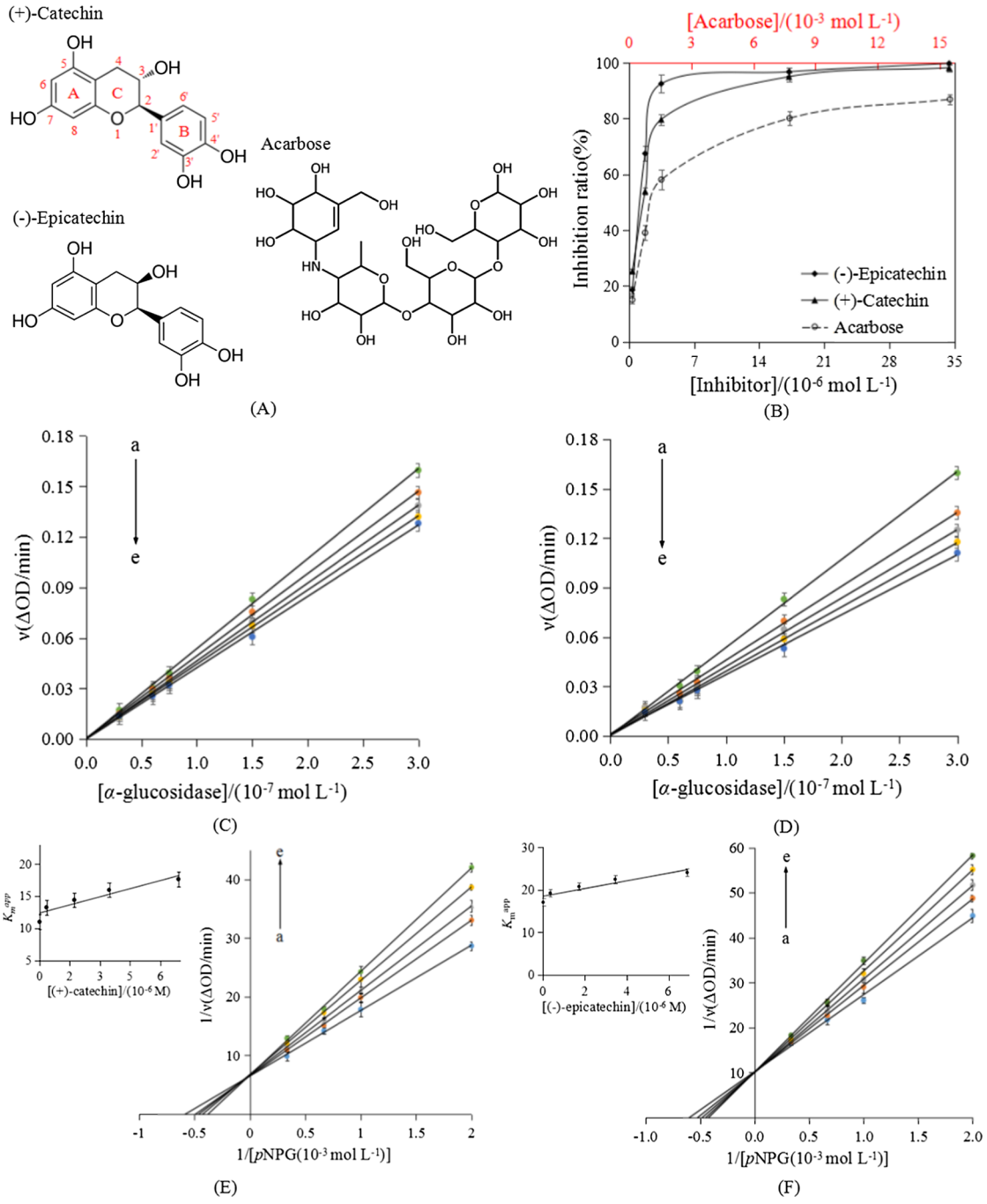

Fig. 1. (A) Structures of C, EC and Acarbose. (B) Inhibitory effects of C, EC and acarbose on AGH (pH 6.8, T = 310 K). c(AGH) = 3×10^{-7} M, and c (pNPG) = 0.3 mM. Plots of ν versus [AGH] for C (C) or EC (D). The ν value shows the change in absorbance at 405 nm at C or EC concentrations between 0 and 6.89×10^{-6} M for curves a–e, respectively. The Lineweaver-Burk plots for C (E) or EC (F). c(C) = c(EC) = (0, 0.34, 1.72, 3.45 and 6.89) $\times 10^{-6}$ M for curves a–e, respectively. The secondary plot represents K_m vs. [C] or [EC] were inserted, respectively.

constants, as well as the number of binding sites [33]. Only the aromatic amino acid residues Trp, tyrosine (Tyr), and phenylalanine emit fluorescence [34]. Given our results suggesting that C and EC inhibit enzyme activity by being bound in the AGH active site, we performed fluorescence spectroscopy to characterize enzyme/inhibitor binding. As show in Fig. 2A and B, addition of C or EC caused gradual decreases in the fluorescence-emission peaks of AGH at 339 nm, and EC binding specifically resulted in a red shift in the maximum emission spectra of AGH, indicating that EC caused a change in AGH conformation, whereas C binding resulted in normal quenching of intrinsic fluorescence.

We then performed static and dynamic fluorescence quenching experiments [33]. In dynamic quenching, increasing the reaction temperature increases the diffusion coefficient and accelerates molecular motion, thereby increasing the quenching constant; however, for static quenching, increased reaction temperature disrupts the stability of the formed complexes, thereby reducing the quenching constant. Stern–Volmer plots describing c-)or EC)-induced quenching of AGH at three different temperatures (298, 304, and 310 K) are presented in Fig. 2A and 2B, with Ksv and Ka values listed in Table 1. The results showed that the Ksv and Ka values for the interaction between C (or EC) and AGH decreased along with increasing temperature. These results indicated that fluorescence quenching was primarily a static process resulting from the formation of the C (or EC)/AGH complex.

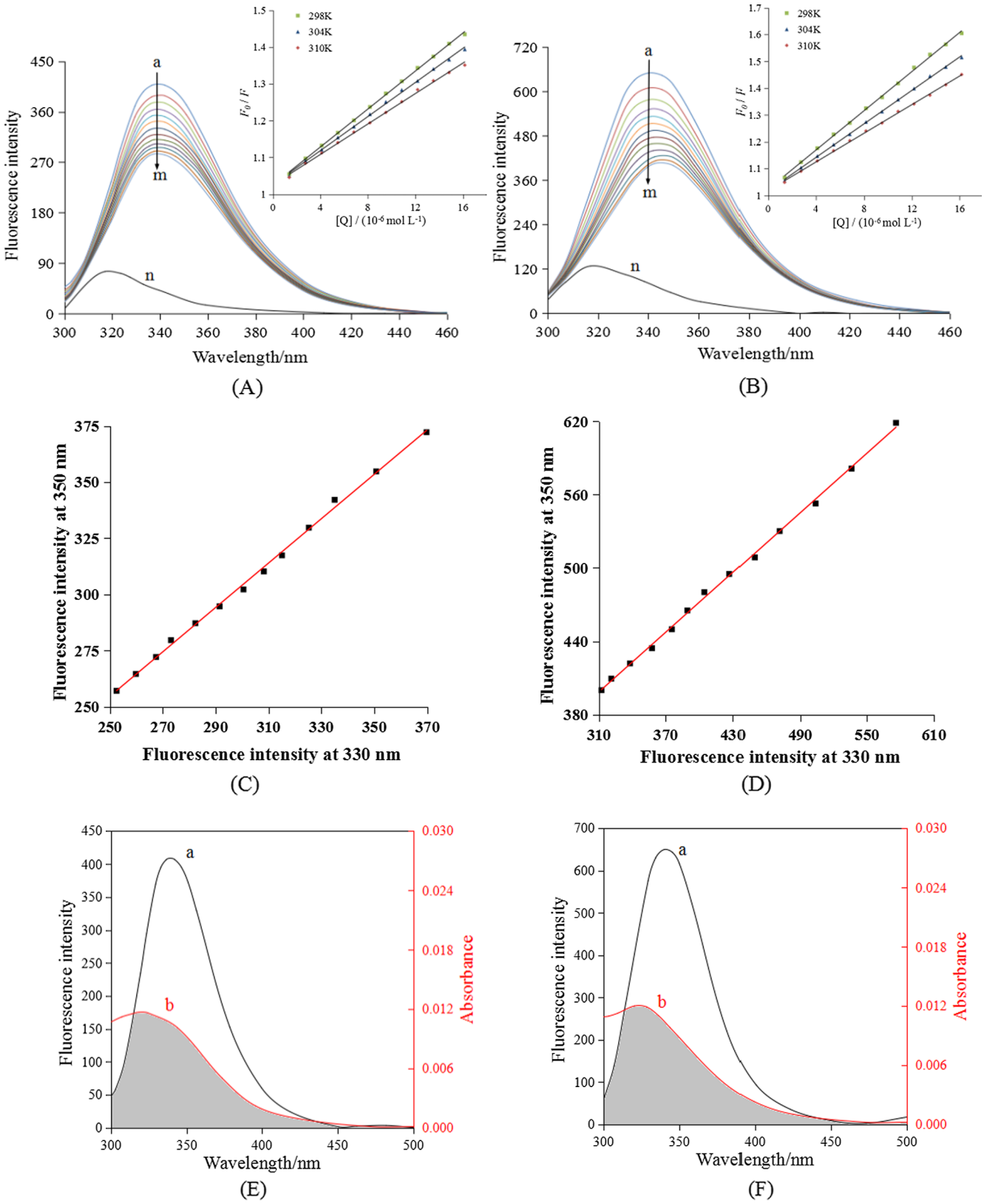

Fig. 2. Effect of C (A) or EC (B) on fluorescence spectra of AGH (A = 1.0×10^{-6} M, B = 2.0×10^{-6} M) at 298 K. c(C) = c(EC) = (0, 1.38, 2.75, 4.11, 5.47, 6.82, 8.17, 9.51, 10.85, 12.18, 13.51, 14.83 and 16.17) × 10^{-6} M for curves a–m, respectively. Curve n shows the emission spectrum of C (A) or EC (B) only. Stern–Volmer plots for the fluorescence quenching of AGH by C or EC at different temperatures were inserted, respectively. Phase diagram of fluorescence of AGH with different concentrations of C (C) or EC (D) at pH 6.8 and T = 298 K. c(C) = c(EC) = (0, 1.38, 2.75, 4.11, 5.47, 6.82, 8.17, 9.51, 10.85, 12.18, 13.51, 14.83 and 16.17) × 10^{-6} M. (E) Spectral overlaps of the fluorescence spectrum of AGH (a) with the absorption spectrum of C, c(AGH) = c(C) = 1.0×10^{-6} M. (F) Spectral overlaps of the fluorescence spectrum of AGH (a) with the absorption spectrum of EC, c(AGH) = c(EC) = 2.0×10^{-6} M.

Table 1
The quenching constants (K_{SV}), binding constants (K_a), number of binding sites (n) and relative thermodynamic parameters for the interaction between C (or EC) and α-glucosidase at different temperatures.

	T (K)	K_{SV} ($\times 10^4$ L mol^{-1})	R^a	K_a ($\times 10^4$L mol^{-1})	n	R^b	ΔH° (kJ mol^{-1})	ΔG° (kJ mol^{-1})	ΔS° (J mol^{-1} K^{-1})
C	298	3.03 ± 0.04	0.99	3.35 ± 0.02	0.98 ± 0.03	0.99	−10.52 ± 0.01	−26.20 ± 0.01	52.61 ± 0.02
	304	2.77 ± 0.04	0.99	2.93 ± 0.01	0.99 ± 0.01	0.99		−26.52 ± 0.01	
	310	2.51 ± 0.03	0.99	2.46 ± 0.01	1.04 ± 0.01	0.99		−26.83 ± 0.01	
EC	298	4.07 ± 0.03	0.99	4.35 ± 0.04	0.98 ± 0.01	0.99	−23.03 ± 0.01	−26.77 ± 0.01	12.54 ± 0.01
	304	3.43 ± 0.02	0.99	3.71 ± 0.02	0.99 ± 0.02	0.98		−26.84 ± 0.01	
	310	2.99 ± 0.02	0.99	3.24 ± 0.01	1.04 ± 0.02	0.99		−26.92 ± 0.01	

R^a is the correlation coefficient for the K_{SV} values. R^b is the correlation coefficient for the K_a values. The values of K_{SV} and K_a were significantly different ($p < 0.05$) from each other in the same column.

Moreover, the number (n) of C- (or EC)-binding sites in AGH at different temperatures was calculated at ~1, suggesting a single inhibitor-binding site in AGH and supporting the data generated by the Lineweaver–Burk plot.

3.4. Synchronous fluorescence spectroscopy

Trp and Tyr residues emit fluorescence spectra at Δλ = 60 nm and Δλ = 15 nm, respectively [35], with the maximum emission wavelength of Trp red shifted along with decreasing hydrophobicity of the environment [36]. We found that the fluorescence intensity of Trp and Tyr decreased in the presence of either C or EC (Fig. 3A–D); however, increasing EC concentrations caused a red shift in the maximum emission wavelength, indicating a change in AGH conformation. These results suggested structural alterations in the regions surrounding the Trp and Tyr residues in AGH following EC binding, resulting in their increased exposure to solvent [37].

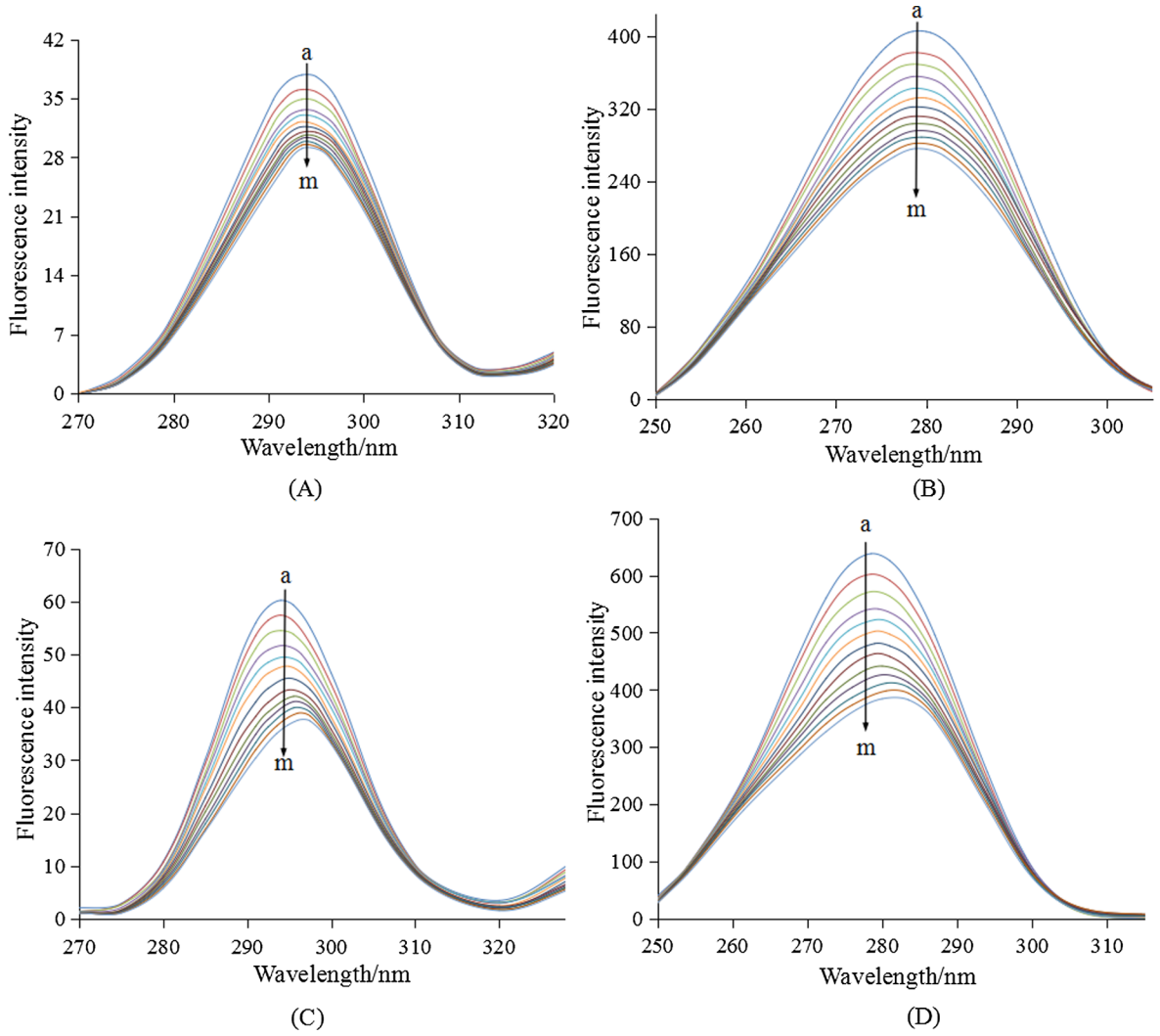

Fig. 3. Synchronous fluorescence spectra of AGH with different concentrations of C, Δλ = 15 nm (A), Δλ = 60 nm (B). Synchronous fluorescence spectra of AGH with different concentrations of EC, Δλ = 15 nm (C), Δλ = 60 nm (D). pH 6.8, T = 298 K, c(AGH) = 2.0 × 10^{-6} M, and c(C) = c(EC) = (0, 1.38, 2.75, 4.11, 5.47, 6.82, 8.17, 9.51, 10.85, 12.18, 13.51, 14.83 and 16.17) × 10^{-6} M for curves a–m, respectively.

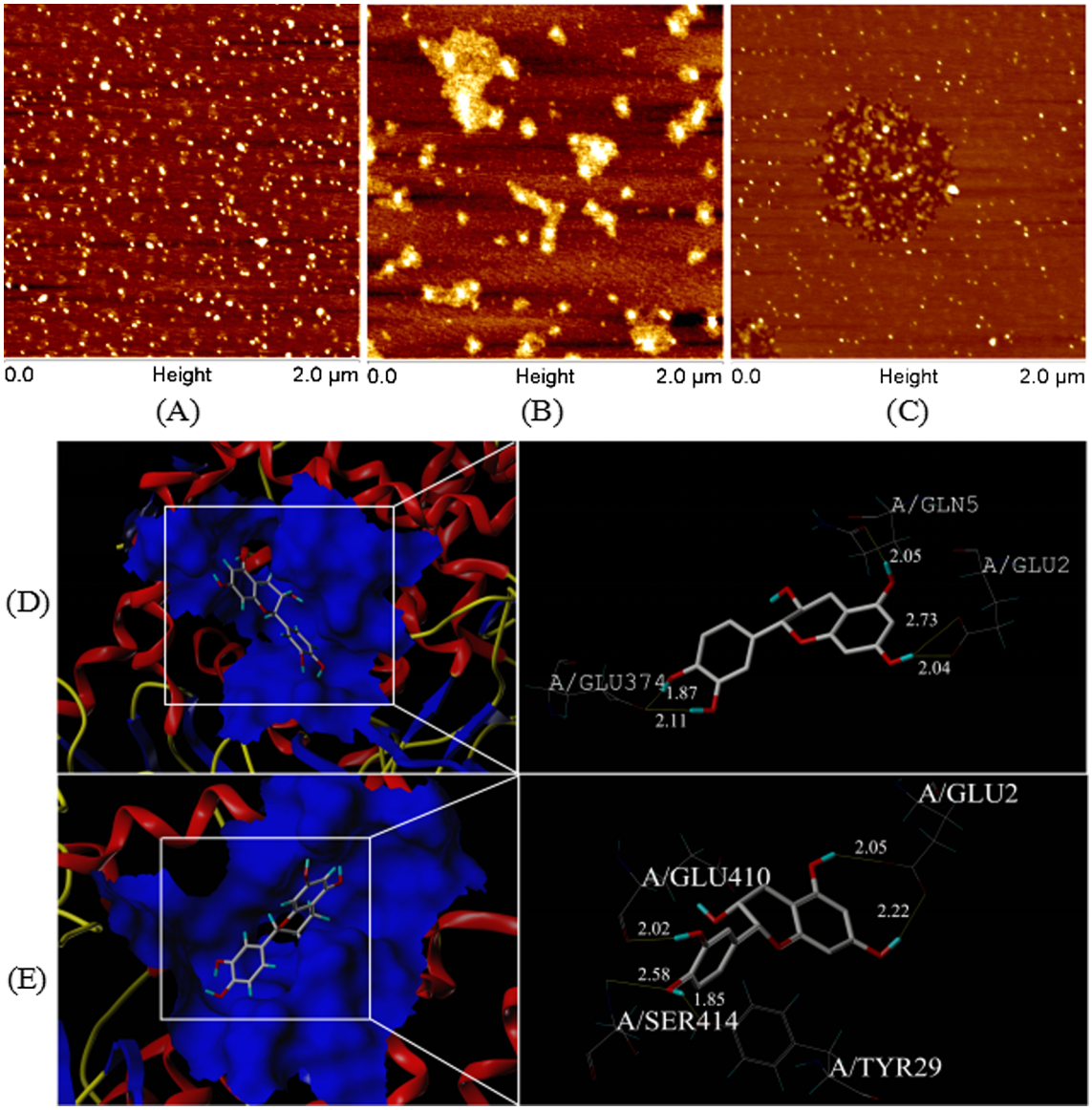

Fig. 4. AFM images of free AGH (A), C-AGH complex (B) and EC-AGH complex (C). c(AGH) = 6.0 × 10^{-7} M, and c(C) = c(EC) = 3.45 × 10^{-5} M. (D) Molecular docking of C with AGH. (E) Molecular docking of EC with AGH. The inhibitor was inserted into the hydrophobic cavity of AGH (blue) in the surface structure (left). Interacted between inhibitor and amino acid residues in the active site of AGH (right). The dashed lines represent hydrogen-bonding interactions.

3.5. Fluorescence phase diagram

Denaturing proteins can attain various degrees of the native state, intermediate state, and unfolded state. Fluorescence phase diagrams generated for AGH in the presence of various concentrations of C or EC (Fig. 2C or D) showed good linearity, implying that AGH transitioned directly from the native state to the unfolded state without attaining a partially folded intermediate state. This findings supported the results describing the inactivation kinetics of inhibitor-bound AGH.

3.6. Thermodynamic analysis

We analyzed the thermodynamic parameters of AGH in order to characterize the binding mode of C (or EC). As shown in Table 1, C or EC binding to AGH represented a spontaneous process based on the negative ΔG values. Additionally, we obtained and ΔH and ΔS of $-10.52 \pm 0.01\,kJ\,mol^{-1}$ and $52.61 \pm 0.02\,J\,mol^{-1}\,K^{-1}$ for C, respectively, $-23.03 \pm 0.01\,kJ\,mol^{-1}$ and $12.54 \pm 0.01\,J\,mol^{-1}\,K^{-1}$ for EC, respectively. These results suggested that electrostatic forces were the predominant factors in C (or EC) binding with AGH [38,39].

3.7. Energy transfer

According to Förster's non-radiative energy transfer theory, and the overlap of the UV–vis spectra of C (or EC) and AGH (Fig. 2E and F), we calculated the following parameters for their interaction: E(C) = 0.3051, E(EC) = 0.3772, R_0(C) = 2.17 nm, R_0(EC) = 2.04 nm, r(C) = 2.48 nm, and r(EC) = 2.22 nm. Given that donor-to-acceptor distance associated with the C (or EC)/AGH complex was < 8 nm (0.5 R_0 < r < 1.5 R_0), these results suggested the high probability of energy transfer from AGH to C (or EC) during binding.

3.8. AFM analysis

AFM analysis of complex formation revealed a free AGH molecule uniformly distributed on the mica in the absence of C (or EC) (Fig. 4A). Fig. 4B shows changes in the image following the addition of C, revealing apparent aggregation of the AGH molecules into sheets, whereas in the presence of EC, AGH aggregated into spherical structures (Fig. 4C).

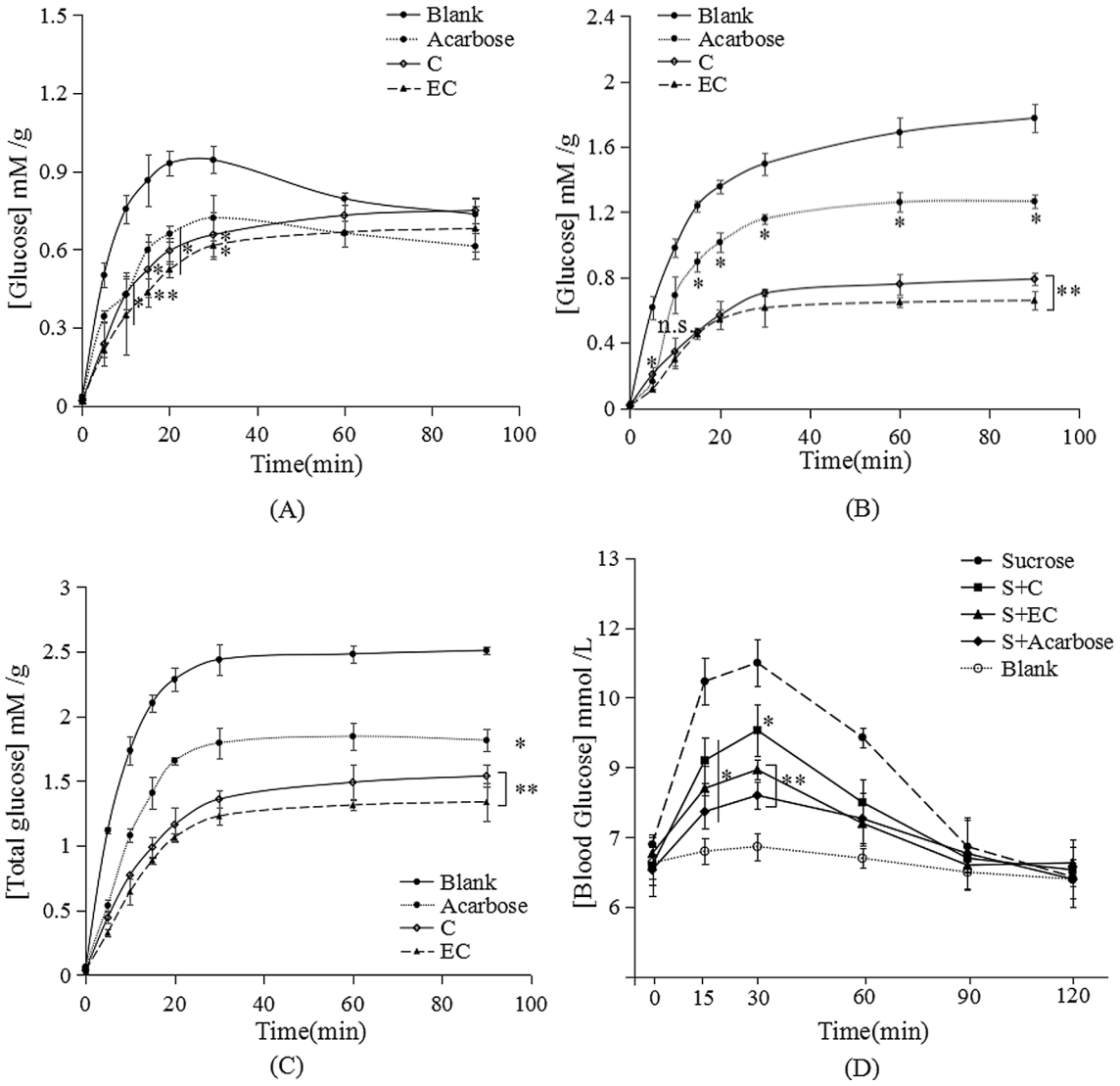

Fig. 5. Glucose uptake in everted intestine sleeves. (A) Glucose concentration in soaking solution. (B) Intestinal sleeves glucose concentration. (C) Total glucose produced by enzymatic hydrolysis. (D) Effect of sucrose load (2 g/kg of body weight) on normal mice in absence of inhibitor and in presence of the same amount of C, EC and acarbose (20 mg/kg body weight). The blank group was the vehicle of 0.5% Carboxymethylcellulose sodium, CMC. Mean values were significantly different from the control: $^{*}P < 0.05$, $^{**}P < 0.01$.

3.9. Molecular docking analysis

Molecular docking analysis revealed that C-binding by AGH involved three hydrogen bonds (Fig. 4D, dashed lines) of lengths ranging from 1.87 Å to 2.73 Å formed between the 5′,7′-dihydroxychromene on the A ring with Gln5 and Glu2 and 4′-hydroxyphenyl on the B ring with Glu374, respectively. Additionally, EC binding in the active site (Fig. 4E) resulted in the formation of four hydrogen bonds (bond distances: 1.85–2.58 Å) between 5′-hydroxychromene on the A ring with Glu2, 3′-hydroxyphenyl on the B ring with Glu410, and 4′-hydroxyphenyl on the B ring with Ser414 and Tyr29. These results suggest that the 4′-hydroxyphenyl on the B ring of flavanols played an important role in AGH inhibition, and that the increased number of residues interacting with the 4′-hydroxyphenyl B ring of EC might enhance the inhibitory effect.

3.10. Inhibition of AGH in a model intestinal environment in vitro

The *in vitro* AGH-inhibitory activity of C, EC, and acarbose was evaluated on sections of everted small intestine by calculating total glucose concentration as the sum of glucose flux on the intestine sleeves (Fig. 5). We found that C and EC were stronger inhibitors of glucose flux than acarbose, and that there were minimal differences in this activity between C and EC. Additionally, we found that C and EC clearly increased the glucose-eflux rate from the intestine sleeves from 15 min to 30 min, thereby altering glucose concentrations in the intestine sleeves. These results implied the potential impact of C- and/or EC-mediated inhibition of intestinal AGH conversion of sucrose to glucose, thereby affecting glucose transport in small-intestinal epithelial cells (data not shown). During carbohydrate digestion and absorption in the small intestine, disaccharides, such as sucrose, are metabolized by AGH into glucose and other monosaccharides, after which glucose enters the blood via glucose transporters on the small intestinal brush border. Therefore, inhibiting AGH activity and that of glucose transporters could significantly attenuate postprandial blood glucose levels and potentially represent a strategy for diabetes treatment [40,41].

3.11. In vivo inhibition of AGH

Because sucrose is the major disaccharide in the human diet, we assessed AGH inhibition by C and/or EC *in vivo* by measuring changes in sucrose loading over time and according to blood glucose levels. As

shown in Fig. 5D, glucose concentration in the blood of the control group did not change significantly at any time point, whereas we observed significant increases that peaked at 30 min following intragastric administration of acarbose. Moreover, administration of C or EC attenuated the observed increases in blood glucose levels from at 15 min to 30 min but with no significant effect on sucrose load relative to the control. These results suggested that C and EC exerted a similar inhibitory effect on AGH as acarbose *in vivo*.

4. Conclusions

In summary, this study examined the antihyperglycemic activity of the flavan-3-ols, C and EC, which were identified as potent AGH inhibitors both *in vitro* and *in vivo*, The results showed that both C and EC showed competitive and reversible inhibition of AGH [IC_{50}: 1.12 ± 0.03 μM and 0.95 ± 0.02 μM, respectively], and that the inhibitory activity of EC was more pronounced than that of C. Fluorescence quenching suggested a static process resulting from the formation of the C (or EC)/AGH complex, and spectral analyses indicated increased solvent exposure of Trp and Tyr residues following EC binding. Moreover, binding of either inhibitor transitioned the enzyme directly from the native to the unfolded state, with conformational changes primarily involving electrostatic forces. Furthermore, AFM studies suggested that inhibitor binding resulted in AGH aggregation, and molecular docking analysis revealed an increased number of hydrogen bonds formed between AGH and EC relative to those observed following C/AGH binding. Importantly, *in vivo* experiments revealed that C and EC effectively reduced levels of postprandial blood glucose via inhibition of AGH activity. These results showed that C and EC exhibited antidiabetic activity *in vitro* and *in vivo* and possess developmental potential as a functional food and antidiabetic drug candidate.

Acknowledgements

This work was supported by the China Agriculture Research System [No. CARS-08-D2-01]; the Science and Industry Coordination Project of Innovation [No. 2017CXY-13].

References

[1] Angelo Avogaro and Gian Paolo Fadini, The effects of dipeptidyl peptidase-4 inhibition on microvascular diabetes complications, Diabetes Care 37 (10) (2014) 2884–2894.
[2] Ismail-Beigi Faramarz, Craven Timothy, Banerji Mary Ann, et al., Effect of intensive treatment of hyperglycaemia on microvascular outcomes in type 2 diabetes: an analysis of the ACCORD randomised trial, Lancet 376 (9739) (2010) 419–430.
[3] R. Pascale, G. Bianco, T.R.I. Cataldi, P.S. Kopplin, F. Bosco, L. Vignola, J. Uhl, M. Lucio, L. Milella, Mass spectrometry-based phytochemical screening for hypoglycemic activity of Fagioli di Sarconi beans (*Phaseolus vulgaris* L.), Food Chem. 242 (2018) 497–504.
[4] H.C. Kadouh, S. Sun, W. Zhu, K. Zhou, α-glucosidase inhibiting activity and bioactive compounds of six red wine grape pomace extracts, J. Funct. Foods 26 (2016) 577–584.
[5] Q. Ong, L. Le, Comparative study on human A-glucosidase, in: 5th International Conference on Biomedical Engineering in Vietnam, 2015, vol. 46, pp. 351–354.
[6] E. Apostolidis, L. Li, L. Chong, N.P. Seeram, In vitro evaluation of phenolic-enriched maple syrup extracts for inhibition of carbohydrate hydrolyzing enzymes relevant to type 2 diabetes management, J. Funct. Foods 3 (2) (2011) 100–106.
[7] D.D. Schmidt, W. Frommer, B. Junge, L. Muller, W. Wingender, E. Truscheit, D. Schafer, α-glucosidase inhibitors-new complex oligosaccharides of microbial origin, Naturwissenschaften 64 (10) (1977) 535–536.
[8] P. Hollander, Safety profile of acarbose, an alpha-glucosidase inhibitor, Drugs 44 (1992) 47–53.
[9] T. Fujisawa, H. Ikegami, K. Inoue, Y. Kawabata, T. Ogihara, Effect of two α-glucosidase inhibitors, voglibose and acarbose, on postprandial hyperglycemia correlates with subjective abdominal symptoms, Metab.-Clin. Exp. 54 (3) (2005) 387–390.
[10] Huiwen Zhang, Yumei Yang, Chaomei Ma, Structures and antioxidant and intestinal disaccharidase inhibitory activities of A-type proanthocyanidins from peanut skin, J. Agric. Food. Chem. 61 (37) (2013) 8814–8820.
[11] Ma. Chao-Mei, Sato Naoto, Li Xiao-Yu, et al., Flavan-3-ol contents, anti-oxidative and α-glucosidase inhibitory activities of Cynomorium songaricum, Food Chem. 118 (1) (2010) 116–119.
[12] D. Gossai, C.A. Laucam, Assessment of the effect of type of dairy product and of chocolate matrix on the oral absorption of monomeric chocolate flavanols in a small animal model, Pharmazie Die 64 (3) (2009) 202–209.
[13] N.T. Zaveri, Green tea and its polyphenolic flavan-3-ol: medicinal uses in cancer and noncancer applications, Life Sci. 78 (18) (2006) 2073–2080.
[14] I. Mcmurrough, M.J. Loughrey, G.P. Hennigan, Content of (+)-catechin and proanthocyanidins in barley and malt grain, J. Sci. Food Agric. 34 (1) (1983) 62–72.
[15] Y. Jin, Y.D. Cheng, K.H. Row, Y.S. Jin, Y.H. Xuan, M.J. Jin, Antioxidation mechanisms of catechin, epicatechin and quercetin using linear solvation energy relationship, Asian J. Chem. 25 (16) (2013) 8863–8866.
[16] M. Yilmazer-Musa, A.M. Griffith, A.J. Michels, et al., Grape seed and tea extracts and catechin 3-gallates are potent inhibitors of alpha-amylase and alpha-glucosidase activity, J. Agric. Food. Chem. 60 (36) (2012) 8924–8929.
[17] J.H. Kim, C.W. Cho, H.Y. Kim, et al., α-Glucosidase inhibition by prenylated and lavandulyl compounds from Sophora flavescens roots and in silico analysis, Int. J. Biol. Macromol. 102 (2017) S0141813017310243.
[18] S. Chen, T. Yong, C. Xiao, J. Su, Y. Zhang, C. Jiao, Y. Xie, Pyrrole alkaloids and ergosterols from Grifola frondosa exert anti-α-glucosidase and anti-proliferative activities, J. Functional Foods 43 (2018) 196–205.
[19] S. Yan, H. Shao, Z. Zhou, Q. Wang, L. Zhao, X. Yang, Non-extractable polyphenols of green tea and their antioxidant, anti-α-glucosidase capacity, and release during in vitro, digestion, J. Funct. Foods 42 (2018) 129–136.
[20] S.R. Park, J.H. Kim, H. Dongjang, S.Y. Yang, Y.H. Kim, Inhibitory activity of minor phlorotannins from Ecklonia cava on α-glucosidase, Food Chem. 257 (2018) 128–134.
[21] X. Peng, G.W. Zhang, Y.J. Liao, D.M. Gong, Inhibitory kinetics and mechanism of kaempferol on alpha-glucosidase, Food Chem. 190 (2016) 207–215.
[22] L. Zeng, G.W. Zhang, S.Y. Lin, D.M. Gong, Inhibitory mechanism of apigenin on alpha-glucosidase and synergy analysis of flavonoids, J. Agric. Food Chem. 64 (37) (2016) 6939–6949.
[23] L. Zhang, X. Zhao, G.J. Tao, J. Chen, Z.P. Zheng, Investigating the inhibitory activity and mechanism differences between norartocarpetin and luteolin for tyrosinase: a combinatory kinetic study and computational simulation analysis, Food Chem. 223 (2017) 40–48.
[24] I.M. Kuznetsova, K.K. Turoverov, V.N. Uversky, Use of the phase diagram method to analyze the protein unfolding-refolding reactions: fishing out the "invisible" intermediates, J. Proteome Res. 3 (3) (2004) 485–494.
[25] S. Bi, L. Yan, Y. Wang, B. Pang, T. Wang, Spectroscopic study on the interaction of eugenol with salmon sperm DNA in vitro, J. Lumin. 132 (9) (2012) 2355–2360.
[26] F.L. Cui, J. Fan, J.P. Li, Z.D. Hu, Interactions between 1-benzoyl-4-p-chlorophenyl thiosemicarbazide and serum albumin: investigation by fluorescence spectroscopy, Bioorg. Med. Chem. 12 (1) (2004) 151–157.
[27] H. Huang, I. Dobryden, P.A. Thoren, L. Ejenstam, J. Pan, M.L. Fielden, D.B. Haviland, P.M. Claesson, Local surface mechanical properties of PDMS-silica nanocomposite probed with Intermodulation AFM, Compos. Sci. Technol. 150 (2017) 111–119.
[28] L. Han, C. Fang, R.X. Zhu, Q. Peng, D. Li, M. Wang, Inhibitory effect of phloretin on alpha-glucosidase: kinetics, interaction mechanism and molecular docking, Int. J. Biol. Macromol. 95 (2017) 520–527.
[29] J. Yan, G. Zhang, J. Pan, Y. Wang, α-glucosidase inhibition by luteolin: kinetics, interaction and molecular docking, Int. J. Biol. Macromol. 64 (2014) 213–223.
[30] M.K. Barker, D.R. Rose, Specificity of processing α-glucosidase I is guided by the substrate conformation: crystallographic and in silico studies, J. Biol. Chem. 288 (19) (2013) 13563–13574.
[31] L. Gomez, E. Molinar-Toribio, M.A. Calvo-Torras, C. Adelantado, M.E. Juan, J.M. Planas, X. Canas, C. Lozano, S. Pumarola, P. Clapes, J.L. Torres, D-Fagomine lowers postprandial blood glucose and modulates bacterial adhesion, Br. J. Nutr. 107 (12) (2012) 1739–1746.
[32] H. Gao, J. Kawabata, Importance of the B ring and its substitution on the alpha-glucosidase inhibitory activity of baicalein, 5,6,7-trihydroxyflavone, J. Agric. Chem. Soc. Jpn. 68 (9) (2004) 1858–1864.
[33] B. Zhang, X. Li, W. Sun, Y. Xing, Z. Xiu, C. Zhuang, Y. Dong, Dietary flavonoids and acarbose synergistically inhibit alpha-glucosidase and lower postprandial blood glucose, J. Agric. Food. Chem. 65 (38) (2017) 8319–8330.
[34] S. Sarzehi, J. Chamani, Investigation on the interaction between tamoxifen and human holo-transferrin: determination of the binding mechanism by fluorescence quenching, resonance light scattering and circular dichroism methods, Int. J. Biol. Macromol. 47 (4) (2010) 558–569.
[35] H. Xiao, B. Liu, H. Mo, G. Liang, Comparative evaluation of tannic acid inhibiting α-glucosidase and trypsin, Food Res. Int. 76 (Pt 3) (2015) 605–610.
[36] M.S. Ali, H.A. Al-Lohedan, Sulfadiazine binds and unfolds bovine serum albumin: an in vitro study, Mol. Biol. Rep. 40 (11) (2013) 6081–6090.
[37] P.B. Kandagal, S. Ashoka, J. Seetharamappa, S.M.T. Shaikh, Y. Jadegoud, O.B. Ijare, Study of the interaction of an anticancer drug with human and bovine serum albumin: spectroscopic approach, J. Pharm. Biomed. Anal. 41 (2) (2006) 393–399.
[38] J. Tian, S. Wei, Y. Zhao, R. Liu, S. Zhao, Studies on interaction between CdTe quantum dots and α-chymotrypsin by molecular spectroscopy, J. Chem. Sci. 122 (3) (2010) 391–400.
[39] P.D. Ross, S. Subramanian, Thermodynamics of protein association reactions: forces contributing to stability, Biochemistry 20 (11) (1981) 3096–3102.
[40] S. Kashanian, M.M. Khodaei, F. Kheirdoosh, In vitro DNA binding studies of Aspartame, an artificial sweetener, J. Photochem. Photobiol., B 120 (2) (2013) 104–110.
[41] H.P. Syama, K.B. Arun, G. Sinumol, R. Dhanya, S. Suseela Anusree, P. Nisha, L. Ravi Shankar, A. Sundaresan, P. Jayamurthy, Syzygium cumini seed exhibits antidiabetic potential via multiple pathways involving inhibition of a-glucosidase, DPP-IV, glycation, and ameliorating glucose uptake in L6 cell lines, J. Food Process. Preserv. (2018) 42 JFPP13464.